

ATOMIC GAS IN BLUE ULTRA DIFFUSE GALAXIES AROUND HICKSON COMPACT GROUPS

KRISTINE SPEKKENS^{1,2} AND ANANTHAN KARUNAKARAN²

¹*Department of Physics
Royal Military College of Canada
PO Box 17000, Station Forces*

Kingston, ON K7K 7B4, Canada
²*Department of Physics, Engineering Physics and Astronomy
Queen's University
Kingston, ON K7L 3N6, Canada*

(Received 2017 Aug 11; Revised 2018 Jan 6; Accepted XXX)

Submitted to ApJ

ABSTRACT

We have found the atomic gas (H I) reservoirs of the blue ultra diffuse galaxy (UDG) candidates identified by Róman and Trujillo in images near Hickson Compact Groups (HCGs). We confirm that all of the objects are indeed UDGs with effective radii $R_e > 1.5$ kpc. Three of them are likely to be gravitationally bound to the HCG near which they project, one is plausibly gravitationally bound to the nearest HCG, and one is in the background. We measure H I masses and velocity widths for each object directly from the spectra, and use the widths together with the UDG effective radii to estimate dynamical masses and halo spin parameters. The location of the blue UDGs in the H I mass – stellar mass plane is consistent with that of the broader gas-rich galaxy population, and both their H I masses and gas richnesses are correlated with their effective radii. The blue UDGs appear to be low-mass objects with high-spin halos, although their properties are not as extreme as those of the faintest diffuse objects found in H I searches. The data presented here highlight the potential of single-dish radio observations for measuring the physical properties of blue diffuse objects detected in the optical.

Keywords: galaxies: distances and redshifts — galaxies: fundamental parameters — galaxies: ISM —
radio lines: galaxies

1. INTRODUCTION

Deep imaging campaigns with both small and large-aperture optical telescopes (e.g. Abraham & van Dokkum 2014; Trujillo & Fliri 2016) have re-invigorated studies of the low surface brightness (LSB) galaxy population (e.g. Impey et al. 1988; Bothun et al. 1991; O’Neil & Bothun 2000). Among the more extreme objects revealed are the ultra diffuse galaxies (UDGs), a population of red ($g - i \sim 0.8$), faint ($\mu_g(0) \gtrsim 24 \text{ mag arcsec}^{-2}$) and extended ($R_e \gtrsim 1.5 \text{ kpc}$) objects in groups and clusters (e.g. van Dokkum et al. 2015; Koda et al. 2015; Yagi et al. 2016; van der Burg et al. 2016, 2017). Since their faintness makes optical spectroscopic follow-up expensive, very few distances or dynamical masses for UDGs have been obtained (Beasley et al. 2016; van Dokkum et al. 2016, 2017; Kadowaki et al. 2017). Nonetheless, a variety of observations suggest that UDGs consist mostly of LSB dwarf galaxies (Beasley & Trujillo 2016; Amorisco & Loeb 2016; Sifón et al. 2017) with an extreme tail of more massive systems (van Dokkum et al. 2016, 2017; Zaritsky 2017).

Optical searches have also revealed populations of blue diffuse objects (James et al. 2015; Román & Trujillo 2017; Shi et al. 2017), while some previously known gas-rich dwarf irregular and LSB galaxies also meet the UDG size and surface brightness criteria (Yagi et al. 2016; Bellazzini et al. 2017; Trujillo et al. 2017). Searches for diffuse stellar counterparts to H I-detected sources have borne fruit as well: Leisman et al. (2017) identify H I-bearing ultra diffuse sources (HUDs) in the ALFALFA 70% catalog (Giovanelli et al. 2005) with similar optical properties to UDGs save for their blue colors. The HUDs appear to be dwarf galaxies embedded in high spin halos.

There may well be an evolutionary connection between diffuse star-forming field objects and red UDGs, with the former being stripped and quenched upon cluster/group infall to resemble the latter. A variety of models posit that the progenitors of red UDGs represent the high-spin tail of the field galaxy population (Yozin & Bekki 2015; Amorisco & Loeb 2016; Rong et al. 2017). On the other hand, Di Cintio et al. (2017) argue that the progenitors are dwarf galaxies that have undergone multiple episodes of gas outflows from star formation, producing a correlation between effective radius and gas richness in these objects. The physical properties of diffuse blue objects therefore place important constraints on the origin of their red counterparts. At the same time, the gas reservoirs of star-forming low surface brightness objects provide an avenue for measuring distances and internal kinematics through the H I spectral line (e.g. Papastergis et al. 2017).

Table 1. Properties of H I spectra

Name	(α, δ) (J2000 deg)	Instr.	δV (km s^{-1})	$\sigma_{\delta V}$ (mJy)	SNR
(1)	(2)	(3)	(4)	(5)	(6)
UDG-B1	(50.09, -1.17)	GBT	10	1.2	15.2
		VLA	21.5	0.6	9.2
UDG-B2	(09.60, +1.11)	GBT	10	0.6	9.0
UDG-B3	(49.96, -0.86)	GBT	10	0.8	10.8
UDG-B4	(09.89, +1.12)	GBT	20	0.4	4.9
UDG-B5	(09.97, +0.38)	GBT	20	1.4	5.8

NOTE—col. (1): name of blue UDG candidate along spectrum LOS, following convention of RT17. col. (2): position of optical feature from RT17. col. (3): for UDG-B1, source of spectrum. cols. (4) and (5): RMS noise $\sigma_{\delta V}$ at spectral resolution δV of spectrum along the LOS in col. (2) and shown in Fig. 1. col. (6): peak signal to RMS noise of feature in spectrum shown in Fig. 1.

Román & Trujillo (2017, hereafter RT17) search for UDGs in SDSS Stripe 82 imaging near Hickson Compact Groups (HCGs, Hickson 1982), uncovering nine objects around HCG07 and HCG25 that satisfy the UDG size and surface brightness criteria. Four of them are red and project within $\sim 250 \text{ kpc}$ of the nearest HCG, and the remaining five are blue and project to larger group-centric distances. Passive evolutionary models applied to the blue UDG candidates produce properties that are broadly consistent with the red ones, suggesting a connection between them. A first step in exploring that connection, however, is to confirm a physical association between the blue UDG candidates and HCGs as well as to measure their basic physical properties.

We have detected the H I reservoirs of the blue UDG candidates identified by RT17 with the Robert C. Byrd Green Bank Telescope (GBT), confirming that they are indeed UDGs with $R_e > 1.5 \text{ kpc}$. We describe the data acquisition and reduction in §2. Our methods for deriving distances and H I masses as well as for estimating dynamical masses and halo spin parameters are explained in §3, where we also compare the blue UDG properties to those of other gas-rich galaxy populations. We describe the implications of our measurements for the structure and evolution of UDGs in §4.

Throughout, we assume distances to HCG07 and HCG25 of 59 Mpc and 88 Mpc, respectively, con-

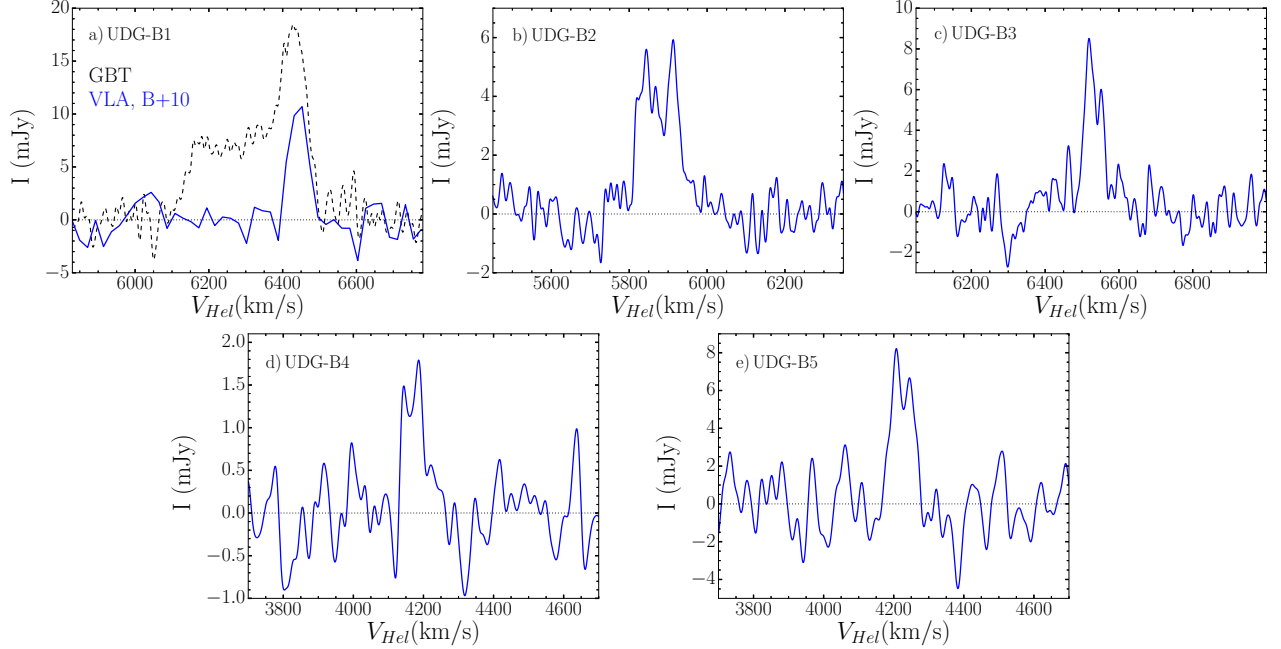


Figure 1. H I detections along the line-of-sight to a) UDG-B1, b) UDG-B2, c) UDG-B3, d) UDG-B4, e) UDG-B5. The RMS noise, spectral resolution and signal-to-noise of each spectrum are given in Table 1. For UDG-B1 in panel a), the GBT spectrum is indicated by the dashed black line, and the VLA spectrum is given by the solid blue line. We use the VLA spectrum in our analysis (see text).

sistent with their recessional velocities and $H_0 = 70 \text{ km s}^{-1} \text{ Mpc}^{-1}$.

2. OBSERVATIONS AND DATA REDUCTION

We obtained five hours of director’s discretionary time on the GBT on 2016 December 28-30 (program AGBT16B-424) to carry out position-switched H I observations of the blue UDG candidates reported by RT17. We used the Versatile GBT Astronomical Spectrometer (VEGAS) with a bandpass of 100 MHz and 3.1 kHz channels, tuned to search for H I at heliocentric recessional velocities in the range $1000 \text{ km s}^{-1} \leq V_{\odot} \leq 21000 \text{ km s}^{-1}$ along the line of sight (LOS) to each UDG candidate and at several reference locations.

Integration times (divided equally between signal and reference locations) for each object were determined by predicting its characteristic H I mass M_{HI} and velocity width using the stellar masses M_* computed by RT17 and the scaling relations of Bradford et al. (2015) for gas-rich field dwarfs. Given our wide bandpass and the distance independence of the ratio M_{HI}/M_* for a feature of fixed spectral width, our observations are sensitive to gas-rich objects in both the foreground and background of the HCG near which each UDG candidate projects on the sky. The $9.1'$ full-width at half-maximum (FWHM) of the GBT at $\nu \sim 1.4 \text{ GHz}$ well exceeds the half-light stellar diameters of the UDG can-

didates, and we therefore expect any H I therein to be detected by a single pointing.

The data were reduced using the standard GBTIDL¹ routine *getps*. We then smoothed the data to different resolutions in the range $10 - 50 \text{ km s}^{-1}$ and examined the resulting spectra for statistically significant emission. We find only one clear H I detection along each LOS. These detections are shown in Fig. 1, with the RMS noise $\sigma_{\delta V}$ at the resolution δV of each spectrum in the figure given in Table 1. We also list the ratio of the peak signal to RMS noise for each feature in Table 1, though its statistical significance is much higher because the emission spans several independent channels.

The spectrum along the LOS to UDG-B1 is much broader and brighter than that of the other targets. It is also the LOS that projects closest to gas-rich HCG 25, raising the possibility of contamination from its brightest group members. We therefore search for emission at the location of UDG-B1 in the $70'' \times 50''$ -FWHM Very Large Array (VLA) maps of HCG 25 presented by Borthakur et al. (2010). We find spatially unresolved H I emission at that location (see Table 1), and the corresponding primary beam-corrected VLA spectrum is presented in Fig. 1a). Compared to our GBT spec-

¹ <http://gbtidl.nrao.edu/>

trum, that from the higher angular resolution VLA is much fainter and narrower. We conclude that the GBT spectrum along that LOS therefore includes a significant contribution from the other HCG 25 group members, and we adopt the VLA spectrum in the analysis of UDG-B1 that follows.

The spectra along the LOS to the blue UDG candidates have shapes characteristic of gas-rich dwarf galaxies, and all but UDG-B1 show hints the double-horned profile expected for a rotating gas-rich disk galaxy (e.g. Giovanelli & Haynes 1988); this is not unexpected given the lower spectral resolution of the VLA data (Table 1). Our detections strongly suggest that we have found the H I reservoirs of the blue UDG candidates. For UDG-B1, the spectrum that we extract from the VLA maps is spatially coincident with the optical feature, and its systemic velocity (§3.1) differs from the SDSS DR13 (SDSS Collaboration et al. 2016) spectroscopic redshift by only 10 km s^{-1} ($\sim 2\sigma$). For UDG-B3, the systemic velocity that we measure is identical within uncertainties to its SDSS DR13 redshift. We searched SDSS imaging and catalogs for potentially gas-rich galaxies within $10'$ (~ 2 GBT beam radii) of the targeted sky position for the other sources that could produce an H I spectrum consistent with that observed, and find none. We therefore conclude that all of our detections are the H I counterparts to the blue UDG candidates identified by RT17.

The distances implied by the centroids of the H I spectra in Fig. 1 confirm that they all have effective radii $R_e > 1.5 \text{ kpc}$ as suggested by RT17 (see §3.2). The candidates are therefore UDGs according to the size criterion of van Dokkum et al. (2015), and we henceforth refer to them as such.

3. H I PROPERTIES OF THE BLUE UDGs

We compute a variety of properties of the blue UDGs from the H I spectra presented in §2, and list the results in Table 2. We focus first on distance-independent quantities that we derive directly from the profiles (§3.1). We then assign a distance to each candidate by comparing its systemic velocity to that of the nearest HCG (§3.2), and use it to compute distance-dependent properties (§3.3).

3.1. Distance-independent quantities

Table 2 presents the heliocentric systemic velocity V_{sys} and the velocity width W_{50} measured for each of the H I detections. We follow the method detailed by Springob et al. (2005) to derive these quantities, fitting a polynomial between 15% and 85% of the peak value f_p of each profile edge minus the spectral RMS noise $\sigma_{\delta V}$

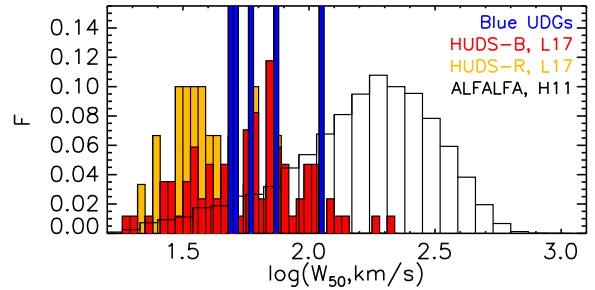


Figure 2. Distribution of W_{50} for the blue UDGs (blue histogram), the HUDs-B (red histogram) and HUDs-R (yellow histogram) samples of H I-bearing ultra diffuse sources from Leisman et al. (2017), and code 1 detections in 40% ALFALFA catalog (unfilled histogram; Haynes et al. 2011).

from Table 1. We define V_{sys} to be the mean of the polynomial fit velocities at the 50% flux level of each edge ($f = 0.5[f_p - \sigma_{\delta V}]$). W_{50} is the difference between these values, corrected for instrumental broadening and cosmological redshift but not for turbulent motions or inclination. As in Springob et al. (2005), uncertainties on W_{50} are dominated by that in the instrumental broadening correction, which we take to be 30% for spectral resolutions $\delta V < 11 \text{ km s}^{-1}$ and 50% otherwise.

Fig. 2 compares the distribution of W_{50} for the blue UDGs to that of the “broad” HUDs-B and “restricted” HUDs-R samples of H I-bearing ultra-diffuse sources reported by Leisman et al. (2017), as well as to code 1 sources in the ALFALFA 40% catalog (Haynes et al. 2011). The values of W_{50} for the blue UDGs are generally commensurate with the HUDs-B distribution, and intermediate to the bulk of the HUDs-R sample and the ALFALFA population. This suggests that their dynamical masses are intermediate to typical values for these two samples as well, though a direct physical interpretation is muddled by the lack of disk inclination or gas turbulence corrections to W_{50} . We estimate dynamical masses for the blue UDGs in §3.3.

The integrated line flux $\int S dv$ of each detection is also given in Table 2, where the uncertainty is dominated by the statistical error in the integral. We use this quantity to compute H I masses in §3.3.

3.2. Distances

With V_{sys} measurements in-hand, we proceed to assign distances D to each blue UDG. To do this, we compare the measured V_{sys} to the mean systemic velocity $V_{sys,HCG}$ of the HCG near which each system projects in order to assess the likelihood that it is gravitationally bound to the group.

Table 2. Properties of H I Detections

Name	V_{sys} (km s^{-1})	W_{50} (km s^{-1})	$\int Sdv$ (Jy km s^{-1})	D	HCG	$\log(M_{HI})$ ($\log[M_{\odot}]$)	$\log(M_*)$ ($\log[M_{\odot}]$)	R_e (kpc)	M_{dyn}^{3Re} ($10^9 M_{\odot}$)	λ
(1)	(2)	(3)	(4)	(5)	(6)	(7)	(8)	(9)	(10)	(11)
UDG-B1 ^a	6440 ± 5	50 ± 10	0.6 ± 0.1	88	HCG25	$9.1^{+0.1}_{-0.1}$	$8.34^{+0.06}_{-0.06}$	3.7 ± 0.4	~ 3	~ 0.2
UDG-B3	6533 ± 1	52 ± 2	0.41 ± 0.05	88	HCG25	$8.88^{+0.06}_{-0.07}$	$8.53^{+0.06}_{-0.06}$	3.2 ± 0.3	~ 3	~ 0.2
UDG-B4	4168 ± 3	58 ± 5	0.09 ± 0.03	59	HCG07	$7.9^{+0.1}_{-0.2}$	$7.85^{+0.06}_{-0.07}$	1.7 ± 0.2	~ 2	~ 0.08
UDG-B5	4229 ± 3	73 ± 5	0.5 ± 0.1	59	HCG07	$8.6^{+0.1}_{-0.2}$	$8.34^{+0.06}_{-0.06}$	3.1 ± 0.3	~ 6	~ 0.1
UDG-B2	5873 ± 1	110 ± 2	0.54 ± 0.05	82	...	$8.93^{+0.05}_{-0.06}$	$8.06^{+0.07}_{-0.08}$	2.8 ± 0.3	~ 10	~ 0.05

NOTE—col. (2): heliocentric systemic velocity of H I detection. col. (3): velocity width at 50% of the H I profile peak, corrected for cosmological redshift and for instrumental broadening using the relations of [Springob et al. \(2005\)](#). col. (4): integrated line flux. col. (5): adopted distance to each detection. col. (6): Hickson Compact Group to which detection likely belongs. col. (7): H I mass, computed using Eq. 1 with $\int Sdv$ in col. (4) and D in col. (5). col. (8): stellar mass from RT17, adjusted to D in col. (5). col. (9): Effective radius from RT17, adjusted to D in col. (5). cols. (10) and (11): dynamical mass and spin parameter estimator computed using Eqs. 2 and 3, respectively, with W_{50} in col. (3) and R_e in col. (9).

a) For UDG-B1, H I properties are calculated using the VLA spectrum in Fig. 1.

Fig. 3 plots relative recessional velocity as a function of HCG-centric distance r_{HCG} (assuming D to be equal to that of the nearest HCG) for all galaxies with SDSS DR13 spectroscopic redshifts that fall within $r_{HCG} = 1 \text{ Mpc}$ and $\Delta V_{sys} = 1000 \text{ km s}^{-1}$ of the sky coordinates and systemic velocities of HCG07 (blue circles) and HCG25 (red triangles). For consistency, we use SDSS DR13 redshifts of confirmed group members (filled circles and triangles; [Hickson et al. 1992](#); [Konstantopoulos et al. 2010](#)) to compute $V_{sys,HCG}$ for each HCG. This value then defines $\Delta V = \sqrt{3}(V_{sys} - V_{sys,HCG}) = 0 \text{ km s}^{-1}$ in Fig. 3, where the factor of $\sqrt{3}$ statistically corrects from line-of-sight to 3D space velocities.

In Fig. 3, the red dashed and blue solid lines correspond to the escape velocities $V_{esc}(r)$ of point masses with $M = 1 \times 10^{12} M_{\odot}$ and $M = 7 \times 10^{11} M_{\odot}$ as appropriate for the halos of HCG07 and HCG25, respectively (RT17; [Munari et al. 2013](#)). The stars show the locations of UDG-B1 and UDG-B3 (which project near HCG25) as well as UDG-B4 and UDG-B5 (which project near HCG07). The upward arrow shows r_{HCG} for B2 (which projects near HCG07), whose ΔV places it well above the plot area.

Fig. 3 illustrates that UDG-B1, UDG-B4 and UDG-B5 all have $|\Delta V| < V_{esc}(r_{HCG})$, and as such are likely to be gravitationally bound to the nearest HCG. We therefore set $D = D_{HCG25}$ for UDG-B1 and $D = D_{HCG07}$

for UDG-B4 and UDG-B5. On the other hand, $\Delta V >> V_{esc}(r_{HCG})$ for UDG-B2; it is therefore not physically associated with HCG07. We use the flow model of [Mould et al. \(2000\)](#) and $H_0 = 70 \text{ km s}^{-1} \text{ Mpc}^{-1}$ to compute a distance $D = 82 \text{ Mpc}$, which places it in the background of HCG07 by $\sim 20 \text{ Mpc}$.

The situation is less clear for UDG-B3: while $|\Delta V| > V_{esc}(r_{HCG})$ and $\Delta V < 0$ could imply that it is a foreground object, it is also true that $V_{sys} - V_{sys,HCG} \sim V_{esc}(r_{HCG})$. In other words, UDG-B3 could be gravitationally bound to HCG25 if its line-of-sight velocity is much larger than its tangential velocity relative to the group. We assume that this is the case and set $D = D_{HCG25}$ for UDG-B3, although none of our conclusions change if we instead assign a flow model distance to this system.

3.3. Distance-dependent quantities

With the distance to each blue UDG established, we proceed to compute distance-dependent quantities. The H I mass M_{HI} for each system is given by the standard relation

$$M_{HI} = 2.356 \times 10^5 D^2 \int Sdv \quad M_{\odot} \quad (1)$$

for optically thin gas, where D is in Mpc and $\int Sdv$ is in Jy km s^{-1} . We adopt a distance uncertainty of 5 Mpc,

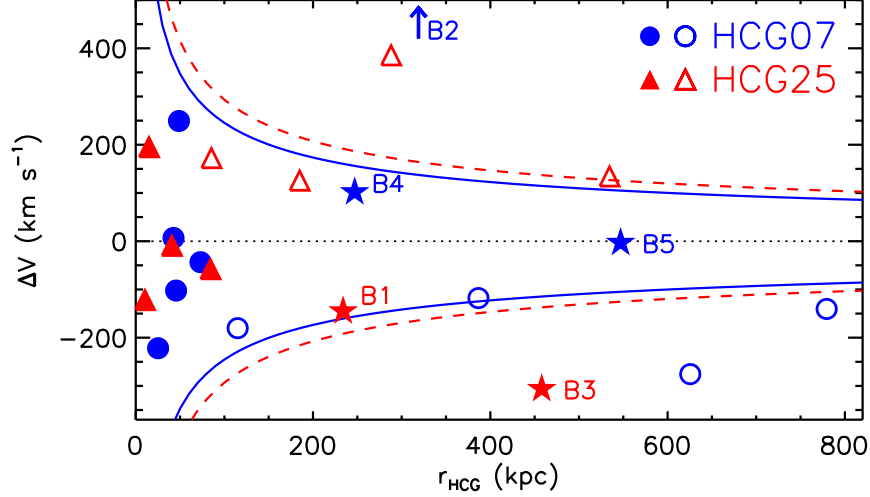


Figure 3. Relative velocities as a function of HCG-centric distance for galaxies with $r_{HCG} < 1$ Mpc (at the group distance) and $\Delta V_{sys} < 1000 \text{ km s}^{-1}$ for HCG07 (blue) and HCG25 (red). Blue circles and red triangles show galaxies with measured velocities near HCG07 and HCG25, respectively, and filled symbols show galaxies used to compute the HCG recessional velocity that corresponds to the horizontal black dotted line at $\Delta V = \sqrt{3}(V_{sys} - V_{sys,HCG}) = 0 \text{ km s}^{-1}$. The blue solid lines and red dashed lines correspond to the escape velocities of point masses with $M = 1 \times 10^{12} M_{\odot}$ and $M = 7 \times 10^{11} M_{\odot}$ appropriate for HCG07 and HCG25, respectively. The stars show the locations of UDG-B1, UDG-B3, UDG-B4 and UDG-B5, and an upward arrow shows r_{HCG} for B2, whose ΔV places it well beyond the plot area.

adding in quadrature with the (dominant) uncertainties on $\int S dv$. The resulting values of $\log(M_{HI})$ are given in Table 2, along with the stellar masses $\log(M_*)$ reported by RT17 and adjusted to our adopted D .

Fig. 4 plots M_{HI} as a function of M_* for the blue UDGs. For comparison, galaxies in the 40% ALFALFA catalog with overlapping SDSS and GALEX coverage that were analyzed by Huang et al. (2012) are shown in grey, galaxies from the Leisman et al. (2017) HUDs-BG sample (the subset of HUDs-B galaxies that are in the Huang et al. 2012 sample) are shown in red, and the blue field UDGs identified by Yagi et al. (2016) and Bellazzini et al. (2017) with estimates of both M_{HI} and M_* in the literature (SdI-1, SdI-2, UGC 2162, UGC 5493, UGC 9024, CGCG 018-057, DDO 87, DDO 143, Malin 1; Hunter & Gallagher 1985; Bottinelli et al. 1990; Pickering et al. 1997; Burkholder et al. 2001; Springob et al. 2005; Cook et al. 2014; Chang et al. 2015; Muñoz-Mateos et al. 2015; Papastergis et al. 2017; Trujillo et al. 2017) are shown in magenta.

We find that the blue UDGs broadly overlap with the ALFALFA 40% population in the $M_{HI} - M_*$ plane, as does the field UDG sample. There is also some overlap between the blue UDGs and the HUDs-BG sample for $\log(M_*) \gtrsim 7.8$, although the former span a larger range in M_{HI} than the latter. This is in part a selection effect caused by the minimum distance imposed

by Leisman et al. (2017) during their search of the ALFALFA 70% catalog.

We list R_e from RT17 for the blue UDGs adjusted to our adopted D in Table 2, and plot M_{HI} and the gas richness M_{HI}/M_* as a function of R_e in Fig. 5. Systems with larger R_e have larger M_{HI} and are more gas-rich, although the correlations are driven largely by the properties of UDG-B4 relative to the other systems.

We use R_e along with W_{50} to estimate dynamical masses for the blue UDGs. Starting from the canonical relation $M = rV^2/G$ for a spherically symmetric system, we assume that the H I distribution extends to $r = 3R_e$ (Broeils & Rhee 1997) and that the rotation velocity at that radius is $V(3R_e) = W_{50}/(2 \sin i)$, where i is the inclination of the H I disk. For simplicity we assume $i = 45^\circ$, which is broadly consistent with the photometric ellipticities measured by RT17. The dynamical mass M_{dyn}^{3Re} , measured within $3R_e$, is then given by:

$$M_{dyn}^{3Re} = 3.5 \times 10^5 R_e W_{50}^2 M_{\odot}, \quad (2)$$

where R_e is measured in kpc and W_{50} is measured in km s^{-1} . We emphasize that, given the assumptions regarding the H I disk extent and the relationship between W_{50} and V_{rot} inherent in Eq. 2, M_{dyn}^{3Re} computed for the blue UDGs and given in Table 2 should be considered as estimates. The dynamical masses of the blue UDGs span a similar range (~ 0.7 dex) to their stellar masses, implying that they are dwarf galaxies.

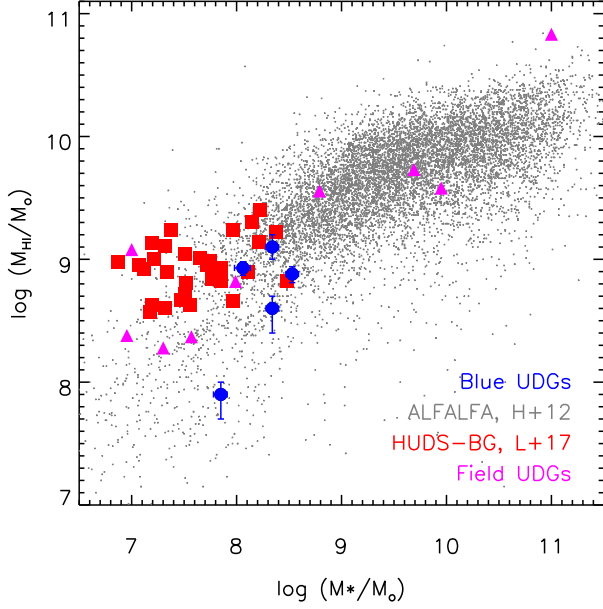


Figure 4. Relationship between HI mass and stellar mass for the blue UDGs (blue circles), galaxies in the 40% ALFALFA catalog with overlapping SDSS and GALEX coverage (Huang et al. 2012, grey points), the HUDS-BG sample of H I-bearing ultra diffuse sources from Leisman et al. (2017, red squares), and the subset of known field UDGs with estimates of M_{HI} and M_* available in the literature.

To gain some insight into the dark matter halos inside which the UDGs may be embedded, we follow Huang et al. (2012) and Leisman et al. (2017) and compute the halo spin parameter estimator from Hernandez et al. (2007). The estimator assumes that galaxies are embedded in self-gravitating, virialized, isothermal dark matter halos that dominate the potential, and that each one has a flat rotation curve with amplitude V_{rot} , an exponential disk with scale-length R_d , and a disk mass fraction $M_*/M_{total} = 0.04$:

$$\lambda = 21.8 \frac{R_d}{V_{rot}^{3/2}} = 21.8 \frac{R_e}{W_{50}^{3/2}}, \quad (3)$$

where the second equality results from converting R_d to R_e for an exponential disk and assuming that $W_{50} = 2V_{rot} \sin i$ with $i = 45^\circ$. While RT17 allow Sérsic n to vary in their photometric models, the best fitting profiles are almost all consistent with $n = 1$ and thus suitable for Eq. 3. The resulting values of λ for the blue UDGs are in Table 2.

We note that even if the numerous assumptions underlying Eq. 3 are correct, the statistical uncertainties on λ are large and the values listed in Table 2 should be interpreted with caution (c.f. Leisman et al. 2017). Nonetheless, they enable comparisons with other samples in which λ is computed in the same way. Fig. 6 presents

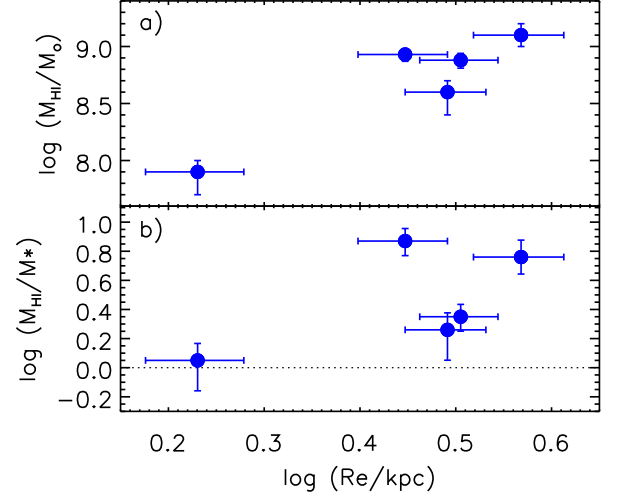


Figure 5. Relationship between effective radius and a) H I mass, and b) gas richness M_{HI}/M_* for blue UDGs.

that comparison, plotting $P(\lambda)d\lambda$ for the blue UDGs, that for the “broad” HUDs-B and “restricted” HUDs-R samples reported by Leisman et al. (2017), as well as the best-fitting lognormal distribution for the ALFALFA 40% sample computed using Eq. 3 (Huang et al. 2012).

The small number of blue UDGs and the large uncertainties on λ imply that standard statistical tests comparing the distributions in Fig. 6 cannot reliably be applied. We instead employ a simpler metric, randomly drawing 10^6 blue UDG-sized samples from the HUDs-R, HUDs-B and ALFALFA $P(\lambda)d\lambda$ and comparing their mean values to that obtained for the blue UDGs. We find that $> 99\%$ of the time, the mean λ of a randomly drawn subset of the HUDs-R (ALFALFA) $P(\lambda)d\lambda$ is larger (smaller) than that of the blue UDGs, even when the blue UDG with the least extreme value relative to that distribution is dropped. On the other hand, randomly-drawn subsamples of the HUDs-B $P(\lambda)d\lambda$ have larger mean values than the blue UDG sample $\sim 40\%$ of the time. This suggests that λ for the blue UDGs are more extreme than those estimated for ALFALFA but less extreme than those from the HUDs-R sample. Instead, they are consistent with being drawn from the HUDs-B sample.

4. DISCUSSION AND CONCLUSIONS

We have found the H I reservoirs of the five blue UDG candidates around HCG07 and HCG25 that were identified by RT17 in optical images. We confirm that all of these objects are indeed UDGs with $R_e > 1.5$ kpc (Fig. 1). Their systemic velocities imply that three of the five UDGs (UDG-B1, UDG-B4 and UDG-B5) are likely to be gravitationally bound to the HCG near

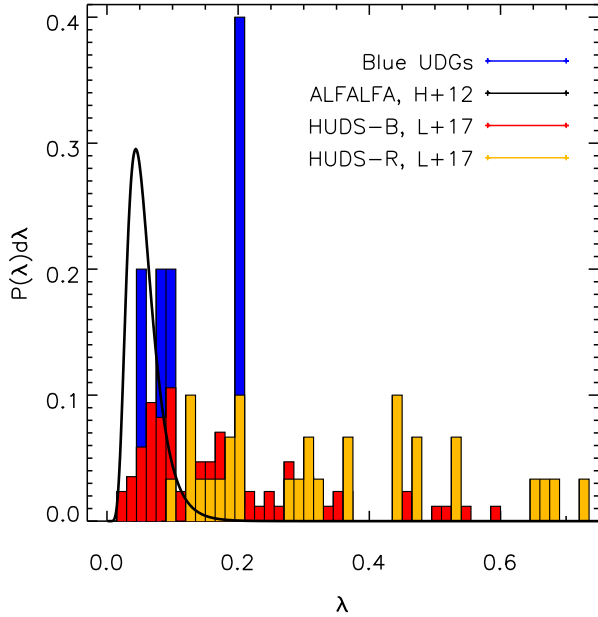


Figure 6. Spin parameter estimator probability distribution $P(\lambda)d\lambda$ for the blue UDGs (blue histogram) as well as the HUDS-B (red histogram) and HUDS-R (yellow histogram) samples of H I-bearing ultra diffuse sources from [Leisman et al. \(2017\)](#). The best-fitting log-normal function to the ALFALFA 40% sample analyzed by [Huang et al. \(2012\)](#) is shown in black. All spins are computed using the estimator in Eq. 3.

which they project, that one (UDG-B3) is plausibly gravitationally bound to HCG25 and that one (UDG-B2) is in the background of HCG07 (Fig. 3).

We use the integrated fluxes, line widths and distances measured from the H I spectra together with the effective radii reported by RT17 to compute H I masses and estimate dynamical masses and spin parameters for the blue UDGs (Table 2). We find that their location in the $M_{HI}-M_*$ plane is broadly consistent with that of the gas-rich galaxy population probed by ALFALFA ([Huang et al. 2012](#)), as well as with other gas-rich UDGs from the literature (Fig. 4). The H I masses and gas fractions of the blue UDGs correlate with their effective radii (Fig. 5). The distribution of their spin parameter estimators appear to be more extreme than those of the broader ALFALFA population, but less so than the “restricted” HUDS-R sample of H I-selected systems from ([Leisman et al. 2017](#)): the latter tend to have narrower velocity widths, higher gas fractions and larger spins than the blue UDGs (Figs. 2, 4 and 6).

Our measures of W_{50} and M_{HI} as well as our estimates of M_{dyn}^{3Re} suggest that the blue UDGs are dwarf galaxies, reminiscent of the low-mass systems thought to make up the bulk of the red UDG population ([Beasley & Trujillo 2016](#); [Amorisco & Loeb 2016](#); [Sifón et al. 2017](#)). Com-

bined with their elevated spins relative to the gas-rich galaxy population probed by ALFALFA, the blue UDGs share similar properties to the H I-selected HUDs ([Leisman et al. 2017](#)). Nonetheless, the blue UDG gas contents and spins are not as extreme as those of the HUDs-R sample; these differences suggest that, as cautioned by [Leisman et al. \(2017\)](#), H I and optical searches may probe different subsets of the LSB galaxy population. We emphasize again that the dynamical masses and halo spin parameter estimators used here are only rough approximations. More reliable measures can be obtained when the H I distribution is resolved ([Hallenbeck et al. 2014](#)); among the objects studied here, only UDG-B1 is a feasible target for higher-resolution interferometric follow-up than presented by [Borthakur et al. \(2010\)](#) and used here in order to obtain the required H I maps.

If the blue UDGs that we confirm to have similar distances to HCG07 and HCG25 do indeed resemble the progenitors of the red UDGs therein, then what constraints do our observations place on models for their origin? The low masses of the blue UDGs as well as the correlation between their effective radii and their H I masses and gas richnesses appear to be consistent with the dwarf galaxy simulations of [Di Cintio et al. \(2017\)](#). This model also predicts that, relative to gas-rich galaxies with similar M_* , the blue UDGs should have an excess of H I but similar halo spins. Instead, our observations suggest that the blue UDGs occupy a similar location in the $M_{HI}-M_*$ plane as the gas-rich galaxy population but have elevated halo spins, as predicted by other UDG formation models ([Yozin & Bekki 2015](#); [Amorisco & Loeb 2016](#); [Rong et al. 2017](#)). It is of course possible that several mechanisms contribute to the formation of UDGs, and that those proposed so far are effective for different subsets of the progenitor population.

The data presented here highlight the potential of single-dish radio telescopes for measuring distances and masses for UDGs identified in the optical, although some care is required to avoid contamination from objects that fall within their relatively broad FWHMs (c.f. UDG-B1). By definition, stellar kinematics of UDGs are expensive to obtain: several hours on 8m-class telescopes are required to secure redshifts for individual objects ([van Dokkum et al. 2015](#); [Kadowaki et al. 2017](#)), and building up sufficient sensitivity to measure a spectral width requires several nights ([van Dokkum et al. 2016, 2017](#)). Such extreme measures are necessary to probe the internal kinematics of gas-poor objects, but the outlook is significantly better for relatively isolated gas-rich ones for which redshifts, H I masses and ve-

locity widths can sometimes be obtained in minutes (Papastergis et al. 2017, this work). Single-dish follow-up is therefore a promising gateway to measuring the physical properties of large samples of UDGs.

We thank Luke Leisman for kindly sharing his data in advance of publication and Sanchayeeta Borthakur for providing her VLA datacube of HCG25. We also thank the referee for a careful consideration of this manuscript and patience with the re-submission process. KS acknowledges support from the National Science and Engineering Research Council of Canada. The GBT is operated by the Green Bank Observatory, which is a facility of the National Science Foundation. This re-

search has made use of the NASA/IPAC Extragalactic Database (NED) which is operated by the Jet Propulsion Laboratory, California Institute of Technology, under contract with the National Aeronautics and Space Administration. Funding for the Sloan Digital Sky Survey IV has been provided by the Alfred P. Sloan Foundation, the U.S. Department of Energy Office of Science, and the Participating Institutions. SDSS-IV acknowledges support and resources from the Center for High-Performance Computing at the University of Utah. The SDSS web site is www.sdss.org.

Facilities: GBT (VEGAS)

REFERENCES

- Abraham, R. G., & van Dokkum, P. G. 2014, *PASP*, 126, 55
- Amorisco, N. C., & Loeb, A. 2016, *MNRAS*, 459, L51
- Beasley, M. A., Romanowsky, A. J., Pota, V., et al. 2016, *ApJL*, 819, L20
- Beasley, M. A., & Trujillo, I. 2016, *ApJ*, 830, 23
- Bellazzini, M., Belokurov, V., Magrini, L., et al. 2017, *MNRAS*, 467, 3751
- Borthakur, S., Yun, M. S., & Verdes-Montenegro, L. 2010, *ApJ*, 710, 385
- Bothun, G. D., Impey, C. D., & Malin, D. F. 1991, *ApJ*, 376, 404
- Bottinelli, L., Gouguenheim, L., Fouque, P., & Paturel, G. 1990, *A&AS*, 82, 391
- Bradford, J. D., Geha, M. C., & Blanton, M. R. 2015, *ApJ*, 809, 146
- Broeils, A. H., & Rhee, M.-H. 1997, *A&A*, 324, 877
- Burkholder, V., Impey, C., & Sprayberry, D. 2001, *AJ*, 122, 2318
- Catinella, B., Giovanelli, R., & Haynes, M. P. 2006, *ApJ*, 640, 751
- Chang, Y.-Y., van der Wel, A., da Cunha, E., & Rix, H.-W. 2015, *ApJS*, 219, 8
- Cook, D. O., Dale, D. A., Johnson, B. D., et al. 2014, *MNRAS*, 445, 899
- Di Cintio, A., Brook, C. B., Dutton, A. A., et al. 2017, *MNRAS*, 466, L1
- Giovanelli, R., & Haynes, M. P. 1988, *Extragalactic neutral hydrogen*, ed. K. I. Kellermann & G. L. Verschuur, 522–562
- Giovanelli, R., Haynes, M. P., Kent, B. R., et al. 2005, *AJ*, 130, 2598
- Hallenbeck, G., Huang, S., Spekkens, K., et al. 2014, *AJ*, 148, 69
- Haynes, M. P., Giovanelli, R., Martin, A. M., et al. 2011, *AJ*, 142, 170
- Hernandez, X., Park, C., Cervantes-Sodi, B., & Choi, Y.-Y. 2007, *MNRAS*, 375, 163
- Hickson, P. 1982, *ApJ*, 255, 382
- Hickson, P., Mendes de Oliveira, C., Huchra, J. P., & Palumbo, G. G. 1992, *ApJ*, 399, 353
- Huang, S., Haynes, M. P., Giovanelli, R., & Brinchmann, J. 2012, *ApJ*, 756, 113
- Hunter, D. A., & Gallagher, III, J. S. 1985, *AJ*, 90, 1789
- Impey, C., Bothun, G., & Malin, D. 1988, *ApJ*, 330, 634
- James, B. L., Koposov, S., Stark, D. P., et al. 2015, *MNRAS*, 448, 2687
- Kadowaki, J., Zaritsky, D., & Donnerstein, R. L. 2017, *ApJL*, 838, L21
- Kalberla, P. M. W., & Kerp, J. 2009, *ARA&A*, 47, 27
- Koda, J., Yagi, M., Yamanoi, H., & Komiyama, Y. 2015, *ApJL*, 807, L2
- Konstantopoulos, I. S., Gallagher, S. C., Fedotov, K., et al. 2010, *ApJ*, 723, 197
- Leisman, L., Haynes, M. P., Janowiecki, S., et al. 2017, *ArXiv e-prints*, arXiv:1703.05293
- Licquia, T. C., & Newman, J. A. 2015, *ApJ*, 806, 96
- Mould, J. R., Huchra, J. P., Freedman, W. L., et al. 2000, *ApJ*, 529, 786
- Muñoz-Mateos, J. C., Sheth, K., Regan, M., et al. 2015, *ApJS*, 219, 3
- Munari, E., Biviano, A., Borgani, S., Murante, G., & Fabjan, D. 2013, *MNRAS*, 430, 2638
- O’Neil, K., & Bothun, G. 2000, *ApJ*, 529, 811
- Papastergis, E., Adams, E. A. K., & Romanowsky, A. J. 2017, *A&A*, 601, L10

- Pickering, T. E., Impey, C. D., van Gorkom, J. H., & Bothun, G. D. 1997, *AJ*, 114, 1858
- Román, J., & Trujillo, I. 2017, *MNRAS*, 468, 4039
- Rong, Y., Guo, Q., Gao, L., et al. 2017, *MNRAS*, 470, 4231
- Salucci, P., Lapi, A., Tonini, C., et al. 2007, *MNRAS*, 378, 41
- SDSS Collaboration, Albareti, F. D., Allende Prieto, C., et al. 2016, *ArXiv e-prints*, arXiv:1608.02013
- Shi, D., Zheng, X., Zhao, H., et al. 2017, *ArXiv e-prints*, arXiv:1708.00013
- Sifón, C., van der Burg, R. F. J., Hoekstra, H., Muzzin, A., & Herbonnet, R. 2017, *ArXiv e-prints*, arXiv:1704.07847
- Springob, C. M., Haynes, M. P., Giovanelli, R., & Kent, B. R. 2005, *ApJS*, 160, 149
- Trujillo, I., & Fliri, J. 2016, *ApJ*, 823, 123
- Trujillo, I., Roman, J., Filho, M., & Sánchez Almeida, J. 2017, *ApJ*, 836, 191
- van der Burg, R. F. J., Muzzin, A., & Hoekstra, H. 2016, *A&A*, 590, A20
- van der Burg, R. F. J., Hoekstra, H., Muzzin, A., et al. 2017, *ArXiv e-prints*, arXiv:1706.02704
- van Dokkum, P., Abraham, R., Brodie, J., et al. 2016, *ApJL*, 828, L6
- van Dokkum, P., Abraham, R., Romanowsky, A. J., et al. 2017, *ApJL*, 844, L11
- van Dokkum, P. G., Abraham, R., Merritt, A., et al. 2015, *ApJL*, 798, L45
- Yagi, M., Koda, J., Komiyama, Y., & Yamanoi, H. 2016, *ApJS*, 225, 11
- Yozin, C., & Bekki, K. 2015, *MNRAS*, 452, 937
- Zaritsky, D. 2017, *MNRAS*, 464, L110